

Electronic and structural properties of Möbius boron–nitride and carbon nanobelts

C. Aguiar¹, N. Dattani^{2,3}, I. Camps^{1,3*}

¹*Laboratório de Modelagem Computacional - LaModel, Instituto de Ciências Exatas - ICEx. Universidade Federal de Alfenas - UNIFAL-MG, Alfenas, Minas Gerais, Brasil*

²*HPQC College, Waterloo, Canada*

³*HPQC Labs, Waterloo, Canada*

Abstract

Using the semiempirical tight binding method as implemented in the xTB program, we characterized Möbius boron–nitride and carbon-based nanobelts with different sizes and compared them with normal nanobelts. The calculated properties include the infrared spectra, the highest occupied molecular orbital (HOMO), the lowest unoccupied molecular orbital (LUMO), the energy gap, the chemical potential, and the molecular hardness. The agreement between the peaks positions from theoretical infrared spectra compared with experimental ones for all systems, validate the used methodology. Our findings show that for the boron–nitride based nanobelts, the calculated properties have opposite monotonic relationship with the size of the systems whereas, for the carbon-based, the properties show the same monotonic relationship for both types of nanobelts. Also, the torsion presented on the Möbius nanobelts, in the case of boron–nitride, induced an inhomogeneous surface distribution for the HOMO orbitals. In all cases, the properties vary with the increase in the size of the nanobelts indicating that it is possible to choose the desired values by changing the size and type of the systems.

Keywords: nanotechnology, nanobelts, boron nitride, carbon

*Corresponding authors

Email addresses: nike@hpqc.org (N. Dattani^{2,3}), icamps@unifal-mg.edu.br (I. Camps^{1,3})

1. Introduction

Carbon (C) can present three different forms of hybridization (sp , sp^2 and sp^3) and the way in which they can combine with other elements is the basis of countless researches [1; 2].

The combination of this element on a nanometric scale gave rise to structures called nanocarbons [3]. They are characterized by showing different geometric and dimensional configurations, such as fullerenes, carbon nanotubes, graphene nanoribbons, graphene oxides and nanodiamonds [1; 4].

Such structures have attracted interest for promising applications in nanobiomedicine [5; 6] and optoelectronics [7; 8]. According to the size and/or different topologies these nanomaterials cause different reactivity in contact with other materials [2; 9], favored or not, according to the geometry of the nanomaterial, which varies according to the increase in the pyramidalization angle and misalignment of the π orbitals between the C atoms [2]. Thus, different syntheses and functionalization have been carried out to obtain different nanostructures to achieve greater compatibility with other materials, seeking to improve and expand nanotechnological applications [5; 9–11].

Povie et al., made a breakthrough with the synthesis of carbon nanobelts (CNBs), whose simple structure in the form of a ring or belt generates two faces, one internal and one external, not convertible to each other [12]. Carbon nanobelts represent segments of single walled carbon nanotubes containing a benzene ring cycle with p orbitals aligned in a plane [13]. Such behavior allows them to be classified as armchair, zigzag or chiral nanoribbons according to the chirality index [13; 14]. In addition to the ring shape, carbon nanobelts are attractive molecules due to their synthetic challenges and differentiated properties [15; 16]. Its formulation covers concepts of conjugation, aromaticity and strain, also providing important information on chirality and bottom-up synthesis of C nanotubes, which continues to be a challenge and has caused limitations in its applications [17]. For the synthesis of nanobelts, three steps must be considered, the first consists of macrocyclization, from carbon sources, the second must occur with the formation of the belt in order to create the double-stranded structure, and finally the induction step stress required to bend the sp^2

hybridized carbon skeleton into a cylindrical topology [12; 18].

But recently, Segawa et al., obtained a new structure, which are structurally uniform, and can be obtained by the bottom-up method in 14 steps of synthesis [17]. These are Möbius carbon nanobelts (MCNBs), whose CNBs structure, when subjected to torsion, should manifest different properties and molecular movements when compared to nanocarbons with a common belt topology [12]. Density functional theory (DFT) calculations show that MCNBs have a higher strain energy than CNBs of the same size [17]. However, producing torsion in CNBs can be difficult to control as strain energy is the major obstacle in the synthesis of MCNBs [12]. For this, saturated ligands ($-\text{CH}_2\text{O}-$) or chalcogen atom ligands ($-\text{S}-$) are used to reduce and control the stress caused by the Möbius shape [19; 20]. Nonetheless, calculations of strain energies showed that MCNBs are synthetically accessible and that strain decreases with increasing MCNBs size [21]. Data from nuclear magnetic resonance spectroscopy and theoretical calculations show that the torsion structure of the Möbius band moves rapidly in solution [17]. Furthermore, chirality arising from the Möbius structure has been demonstrated experimentally using chiral separation by high performance liquid chromatography (HPLC) and circular dichroism (DC) spectroscopy [17]. Besides, spectroscopy data on excitation at 380 nm showed blue-green fluorescence beyond 10% quantum yield [17].

Given the above, new synthetic route strategies, different topologies and varied functionalization, combined with deformation calculations may contribute to the improvement of new nanocarbon materials from CNBs, including Möbius. This would make it possible to properly relate structure and function for applications in several areas. Thus, the objective of this work is to determine the electronic and structural properties of carbon and boron–nitride nanobelts and Möbius nanobelts with different sizes. The knowledge of such properties can help to develop sensors and filters for heavy metal, green house and hazardous gases.

2. Materials and Methods

In this work two type of nanobelts were used for C and B–N systems. The first one consist in nanobelts whereas the second one are Möbius nanobelts (twisted nanobelts). The

structures were generated starting with a cell with 2 units of (10,0) nanosheet repeated N times (10, 15, 20, 25 and 30) in the z direction and then wrapped 360°. After that, the periodicity was removed and the atoms of the borders were passivated with Hydrogen. In case of Möbius nanobelts, after repetition, the nanobelts were twisted 180° and then wrapped. All the structures were generated using the Virtual NanoLab Atomistix ToolKit software [22].

The nomenclature to identify the systems is described as follows. BNNB_N (CNB_N) for boron–nitride (carbon) nanobelts and MBNNB_N (MCNB_N) for Möbius boron–nitride (carbon) nanobelt. In all cases, N indicates the number of repetitions.

Using the semiempirical tight binding method as implemented in the xTB program [23], the electronic and structural parameters were calculated. The calculations were done using the GFN2–xTB method, an accurate self–consistent method that includes multipole electrostatics and density–dependent dispersion contributions [24] with the extreme optimization level that ensures convergence energy of $5 \times 10^{-8} E_h$ and gradient norm convergence of $5 \times 10^{-5} E_h/a_0$ (a_0 is the Bohr radii).

For each optimized structure, the highest occupied molecular orbital, HOMO (ε_H); the lowest unoccupied molecular orbital, LUMO (ε_L); the energy gap ($\Delta\varepsilon$) between HOMO and LUMO orbitals ($\Delta\varepsilon = \varepsilon_H - \varepsilon_L$); the chemical potential (μ); the molecular hardness (η); and the infrared spectra were determined.

Considering the approximation that ignores orbital relaxation after an electron is removed from the system (Koopmans’ s theorem [25–28] together with Janak’ s theorem [29]) it is possible to estimate the chemical potential (μ), the molecular hardness (η) [30], and the electrophilicity index (ω) [31] from the HOMO and LUMO energies ε_H and ε_L as follows:

$$\mu \cong \frac{\varepsilon_L + \varepsilon_H}{2} \quad (1)$$

$$\eta \cong \frac{\varepsilon_L - \varepsilon_H}{2} \quad (2)$$

$$\omega = \frac{\mu^2}{2\eta} \quad (3)$$

3. Results and discussion

Figures 1 and 2 shown the top view of the optimized structures. Panel A shows the nanobelts and panel B shows the Möbius nanobelts. With the increase of repetitions (n), the diameter increase too, starting from 13.81 Å (13.77 Å) to 40.79 Å (40.77 Å) for boron–nitride (carbon) nanobelts. The minimum number of repetition used was 10 to avoid stressed structures.

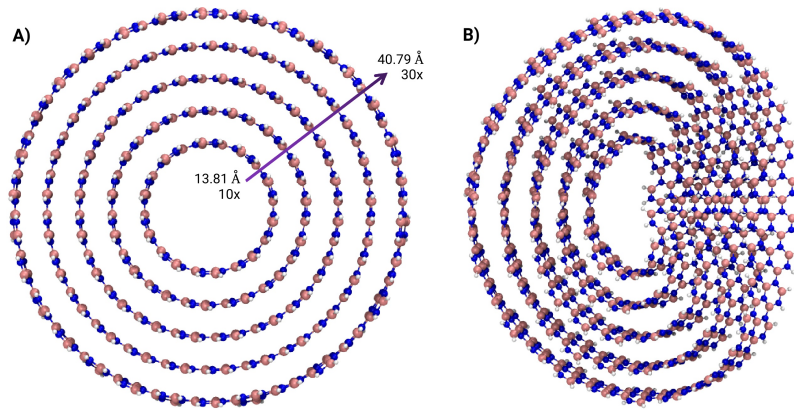


Figure 1: Top view of: A) Boron–nitride nanobelts (BNNB) with minimum/maximum diameter and repetition. B) Möbius boron–nitride nanobelts (MBNNB). Image rendered with VMD [32] software.

The calculated infrared spectra for each system are shown in figures 3 and 4. At first sight (figure 3), the spectra for both systems, BNNB and MBNNB are very similar, indicating that the torsion on the Möbius nanobelts did not appreciable change the principal oscillation modes. In both cases, the B–N stretching (in–plane and out–of–plane) and radial R mode (out–of–plane buckling) are observed. The oscillations around 800 cm^{-1} correspond to the out–of–plane buckling mode. All the resonances in the high–frequency regime above 1200 cm^{-1} consists of transverse optical (T) and longitudinal optical (L) phonon modes. Oscillations around 1200 cm^{-1} and 1380 cm^{-1} correspond to bond–bending or T modes and around 1340 cm^{-1} and 1420 cm^{-1} correspond to bond–stretching or L modes [33–36].

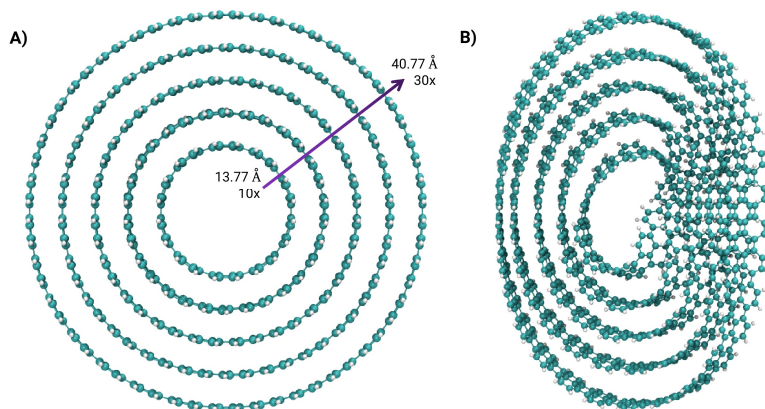
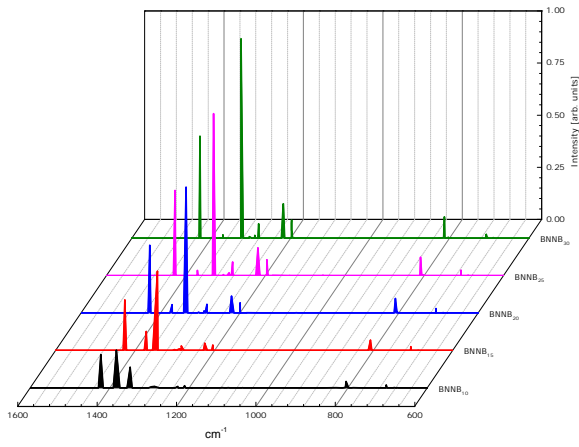


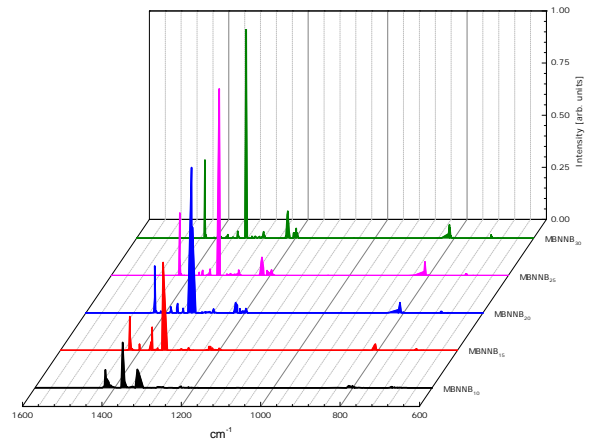
Figure 2: Top view of: A) Carbon nanobelts (CNB) with minimum/maximum diameter and repetition. B) Möbius carbon nanobelts (MCNB). Image rendered with VMD [32] software.

The case for the carbon nanobelts systems, CNB and MCNB, is different. For both systems, the fingerprint region ($600 - 1500 \text{ cm}^{-1}$) is visible but the peaks are with very dissimilar intensities, being greater for the MCNB structures. For carbon based organic systems, the resonances around $900 - 675 \text{ cm}^{-1}$ consist on out-of-plane C–H oscillation, around $1500 - 1400 \text{ cm}^{-1}$ were identified as C–C stretch (in-ring modes), and around $3100 - 3000 \text{ cm}^{-1}$, as C–H bond stretch [37]. These results indicate that the MCNB are more freely to oscillate than the CNB.

The electronic properties for boron–nitride and carbon based systems are shown in figures 5. Figures 5(a) and 5(b) show the energies of HOMO and LUMO boundary orbitals. To some extent, from the energies of these orbitals, it is possible to know how reactive the system is. The electron–donor character (electron–donor capacity) is measured by the HOMO energy whereas the electron–acceptor character (resistance to accepting electrons) is measured by the LUMO energy. From these figures, we can see that, in case of HOMO energy, the BNNB and MBNNB have opposite behavior. With the increase of the number of repeat units, the capacity to donate electrons is decreased for the MBNNB system and increased for the BNNB. On the other hand, the behavior of LUMO energy with the increase

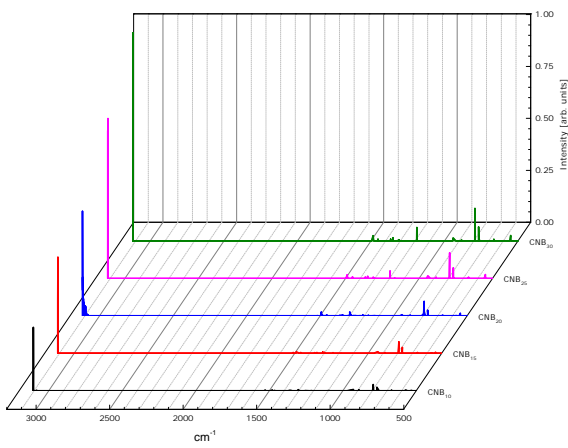


(a) BNNB system

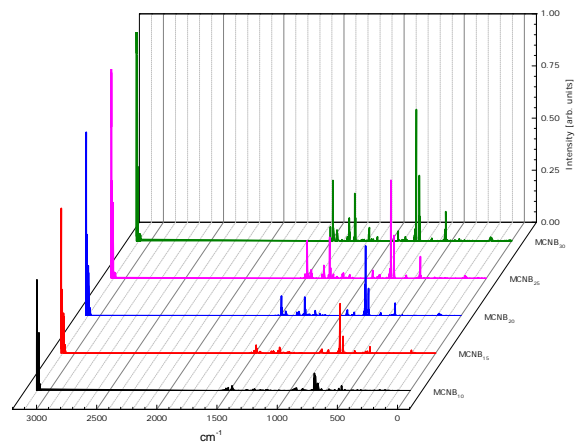


(b) MBNNB system

Figure 3: Calculated infrared spectra for boron–nitride nanobelts.



(a) CNB system



(b) MCNB system

Figure 4: Calculated infrared spectra for carbon nanobelts.

of systems size is similar, increasing the resistance to accept electrons.

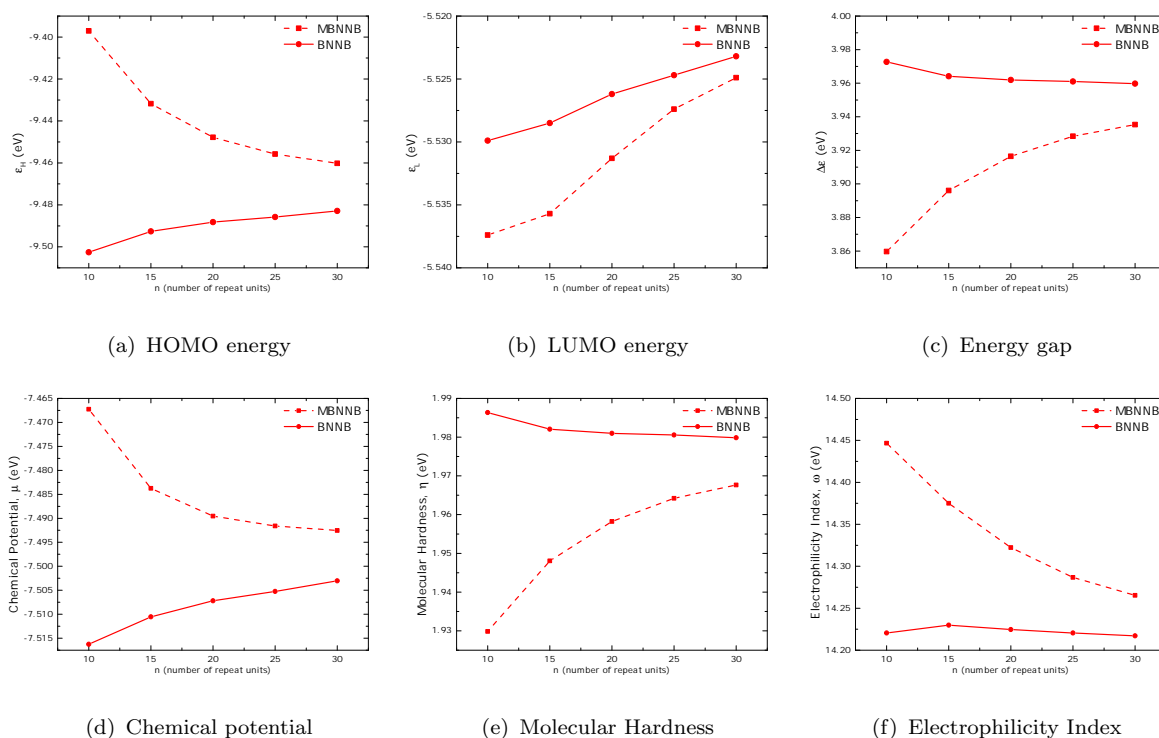


Figure 5: Calculated electronic properties for boron-nitride nanobelts.

Top view of the 3-D diagrams of the HOMO and LUMO surfaces for the BNNB₂₀ and MBNNB₂₀ are shown in figures 6 (the 3-D diagrams for all the structures are shown in figures S1 and S2 of Supplementary material). The distribution of HOMO and LUMO surfaces for the BNNB are, as expected, in accordance with the symmetry of the system being distributed homogeneously over all the structure. In case of the MBNNB, the torsion on the nanobelt induced an strain on the structure that in turn, modify how the orbitals are distributed. This modification is stronger for the HOMO where the orbital volume is redistributed having regions with smaller/greater volumes. As the volume of the orbitals are proportional to the probability to find the electrons, the electron-donor regions changed too, with low/high localized HOMO zones. On the other hand, the LUMO surface shows very little inhomogeneities. This behavior is the same for all the MBNNB as shown in figure S2.

The gap ($\Delta\epsilon$), chemical potential (μ), molecular hardness (η), and electrophilicity index (ω) can be used to estimate the chemical reactivity and hardness of the system together with

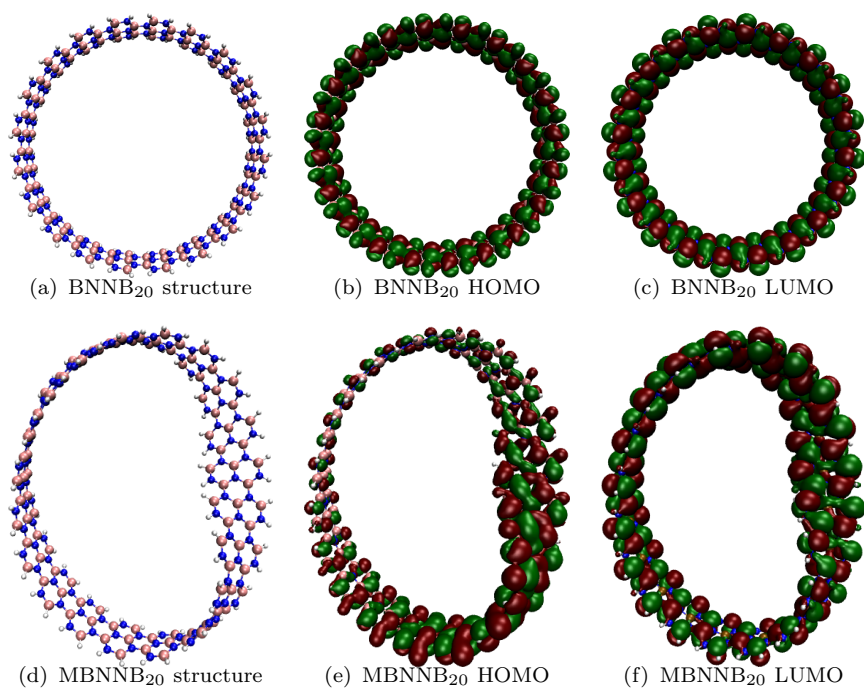


Figure 6: Structures, HOMO and LUMO surfaces for BNNB₂₀ and MBNNB₂₀ systems. Red (green) color represents negative (positive) values. Orbital surfaces rendered with with isovalue equal to 0.001 and with VMD [32] software.

its molecular stability. Molecules with high (low) gap are those with high (low) molecular stability [38]. Positive values for η indicates that the redistribution of electrons in the molecule is energetically unfavorable. Also, the higher η value is, the more chemically stable the molecule is and, therefore, harder the rearrangement of its electrons [39]. The electrophilicity index (ω), can be used as a measure of the molecule energy lowering due to the maximal electron flow between the environment and the molecule [31].

Comparing the values of $\Delta\varepsilon$, μ , η and ω for BNNB and MBNNB systems, we can see that the values are on the same order of magnitude. The main difference is in how these properties change with the increase of the number of repeated units used to build the nanobelts. These can be used to design structures with a fine control of these properties.

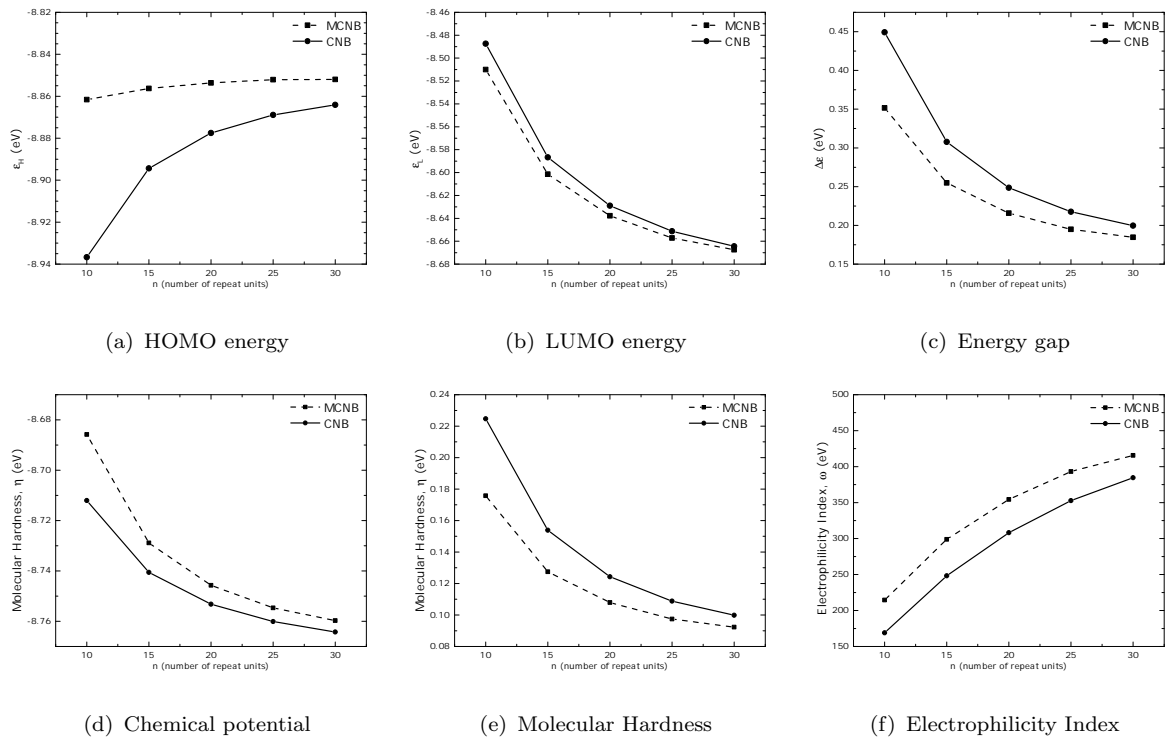


Figure 7: Calculated electronic properties for carbon nanobelts.

Figure 7 shows the electronic properties for the carbon nanobelts. All the graphs shown a different behavior when compare to boron–nitride nanobelts. In this case, the properties for both systems, CNB and MCNB, behave with the same monotonic variation.

The 3–D top view diagrams of the HOMO and LUMO surfaces for the CNB₂₀ and

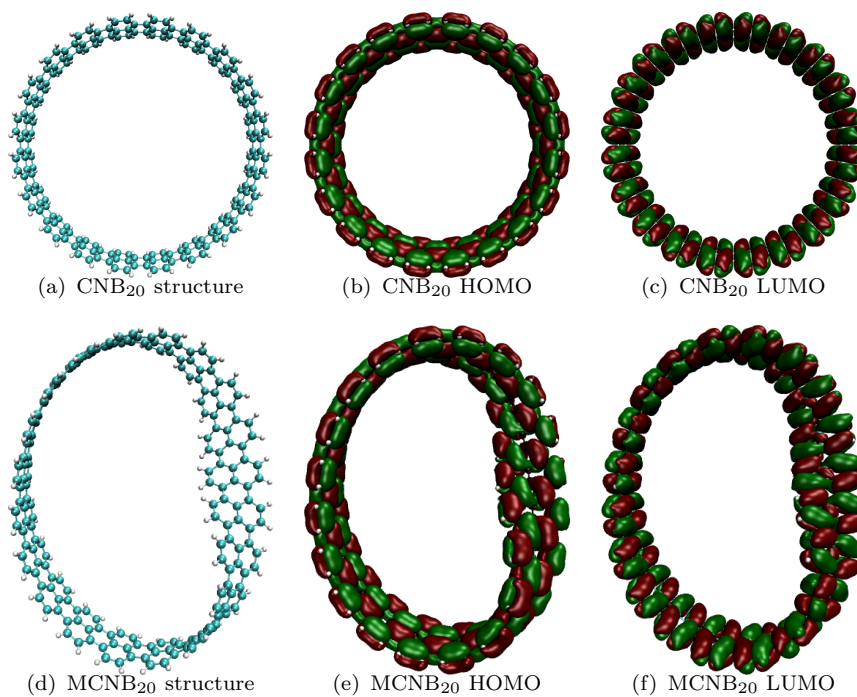


Figure 8: Structures, HOMO and LUMO surfaces for CNB₂₀ and MCNB₂₀ systems. Red (green) color represents negative (positive) values. Orbital surfaces rendered with with isovalue equal to 0.001 and with VMD [32] software.

MCNB₂₀ are shown in figures 8 (the 3-D diagrams for all the structures are shown in figures S3 and S4 of Supplementary material). In this case, the torsion on the nanobelt did not modify substantially either orbitals surfaces for any system.

The values of $\Delta\varepsilon$, μ , η and ω for CNB and MCNB systems, are similar among them having small variations with the increase of the number of repeat units used to build the nanobelts. As the properties also vary with the increase of repeat units, the change in n can tailor the electronic properties of the carbon nanobelts.

The inhomogeneous distribution of the HOMO surfaces can be correlated with the molecular hardness, η . As η is related with how energetically unfavorable is to redistribute the electrons in a molecule, higher values implies a harder rearrangement of them. Comparing the values of η for the MBNNB (5(e)) and MCNB (7(e)) systems, we can see that η is almost eight times bigger for boron–nitride nanobelts than for carbon based nanobelts. A lower value of η imply that the electrons can redistribute easily through the whole structure resulting in a more homogeneous HOMO surface.

4. Conclusions

In this work we studied the structural and electronic properties of boron–nitride and carbon based Möbius nanobelts and compare their properties with simple nanobelts. For all systems, the main peaks in the infrared calculated spectra are in accordance with the experimental one, indicating that the theoretical methodology used here is suitable to determine other properties.

The electronic properties shown differences between both boron–nitride nanobelts. Whereas the LUMO energy for both systems, BNNB and MBNNB, have similar monotony, the other properties shown opposite behavior (different monotony). All the properties for the carbon based nanobelts have the same monotonic behavior for all the properties. Finally, the inhomogeneous distribution of the HOMO surface for the MBNNB was related with the high values of the molecular hardness. In all cases, the properties vary with the increase of the number of repeat units indicating that it is possible to choose the desired values changing the size and type of the systems.

Acknowledgements

We would like to acknowledge financial support from the Brazilian agencies CNPq, CAPES and FAPEMIG. Part of the results presented here were developed with the help of a CENAPAD-SP (Centro Nacional de Processamento de Alto Desempenho em São Paulo) grant UNICAMP/FINEP–MCT, CENAPAD–UFC (Centro Nacional de Processamento de Alto Desempenho, at Universidade Federal do Ceará), and Digital Research Alliance of Canada (via project bmh-491-09 belonging to Dr. Nike Dattani), for the computational support.

References

- [1] N. S. Kasálková, P. Slepíčka, V. Švorčík, Carbon nanostructures, nanolayers, and their composites, *Nanomaterials* 11 (2021) 2368 (2021). doi:10.3390/nano11092368.
- [2] M. C. G. Pedrosa, J. C. D. Filho, L. R. de Menezes, E. O. da Silva, Chemical surface modification and characterization of carbon nanostructures without shape damage, *Materials Research* 23 (2020) e20190493 (2020). doi:10.1590/1980-5373-MR-2019-0493.
- [3] H. Jirimali, J. Singh, R. Boddula, J. Lee, V. Singh, Nano-structured carbon: Its synthesis from renewable agricultural sources and important applications, *Materials* 15 (2022) 3969 (2022). doi:10.3390/ma15113969.
- [4] Y. Segawa, M. Kuwayama, Y. Hijikata, M. Fushimi, T. Nishihara, J. Pirillo, J. Shirasaki, N. Kubota, K. Itami, Topological molecular nanocarbons: All-benzene catenane and trefoil knot, *Science* 365 (2019) 272–276 (2019). doi:10.1126/science.aav5021.
- [5] K. Y. Cheung, Y. Segawa, K. Itami, Synthetic strategies of carbon nanobelts and related belt-shaped polycyclic aromatic hydrocarbons, *Chem. Eur. J.* 26 (2020) 14791–14801 (2020). doi:10.1002/chem.202002316.
- [6] N. Panwar, A. M. Soehartono, K. K. Chan, S. Zeng, G. Xu, J. Qu, P. Coquet, K. Yong, X. Chen, Nanocarbons for biology and medicine: Sensing, imaging, and drug delivery, *Chem. Rev.* 119 (1) (2019) 9559–9656 (2019). doi:10.1021/acs.chemrev.9b00099.
- [7] N. Saba, M. Jawaid, H. Fouad, O. Y. Allothman, *Nanocarbon: Preparation, properties, and applications*, Elsevier, 2019 (2019). doi:10.1016/B978-0-08-102509-3.00009-2.
- [8] C. J. Shearer, L. Yu, J. G. Shapter, *Synthesis and applications of nanocarbons*, Wiley, 2020, Ch. Optoelectronic properties of nanocarbons and nanocarbon films, pp. 275–294 (2020). doi:10.1002/9781119429418.ch9.

- [9] K. Itami, T. Maekawa, Molecular nanocarbon science: Present and future, *Nano Lett.* 20 (2020) 4718–4720 (2020). doi:10.1021/acs.nanolett.0c02143.
- [10] Q. Guo, Y. Qiu, M. Wang, J. F. Stoddart, Aromatic hydrocarbon belts, *Nat. Chem.* 13 (2021) 402–419 (2021). doi:10.1038/s41557-021-00671-9.
- [11] F. Yang, M. Wang, D. Zhang, J. Yang, M. Zheng, Y. Li, Chirality pure carbon nanotubes: Growth, sorting, and characterization, *Chem. Rev.* 120 (2020) 2693–2758 (2020). doi:10.1021/acs.chemrev.9b00835.
- [12] G. Povie, Y. Segawa, T. Nishihara, Y. Miyauchi, K. Itami, Synthesis of a carbon nanobelt, *Science* 356 (2017) 172–175 (2017). doi:10.1126/science.aam8158.
- [13] Z. Xia, S. H. Pun, H. Chen, Q. Miao, Synthesis of zigzag carbon nanobelts through scholl reactions, *Angew. Chem.* 133 (2021) 10399–10406 (2021). doi:10.1002/ange.202100343.
- [14] T. W. Price, R. Jasti, Carbon nanobelts do the twist, *Nature Synthesis* 1 (2022) 502–503 (2022). doi:10.1038/s44160-022-00083-8.
- [15] X. Lu, J. Wu, After 60 years of efforts: The chemical synthesis of a carbon nanobelt, *Chem* 2 (2017) 619–620 (2017). doi:10.1016/j.chempr.2017.04.012.
- [16] H. Chen, Q. Miao, Recent advances and attempts in synthesis of conjugated nanobelts, *J. Phys. Org. Chem.* 33 (2020). doi:10.1002/poc.4145.
- [17] Y. Segawa, T. Watanabe, K. Yamanoue, M. Kuwayama, K. Watanabe, J. Pirillo, Y. Hijikata, K. Itami, Synthesis of a Möbius carbon nanobelt, *Nature Synthesis* 1 (2022) 535–541 (2022). doi:10.1038/s44160-022-00075-8.
- [18] Y. Li, H. Kono, T. Maekawa, Y. Segawa, A. Yagi, K. Itami, Chemical synthesis of carbon nanorings and nanobelts, *Acc. Mater. Res.* 2 (2021) 681–691 (2021). doi:10.1021/accountsmr.1c00105.
- [19] S. Nishigaki, Y. Shibata, A. Nakajima, H. Okajima, Y. Masumoto, T. Osawa, A. Muranaka, H. Sugiyama, A. Horikawa, H. Uekusa, H. Koshino, M. Uchiyama, A. Sakamoto, K. Tanaka, Synthesis of belt- and Möbius-shaped cycloparaphenylenes by rhodium-catalyzed alkyne cyclotrimerization, *J. Am. Chem. Soc.* 141 (2019) 14955–14960 (2019). doi:10.1021/jacs.9b06197.
- [20] S. Wang, J. Yuan, J. Xie, Z. Lu, L. Jiang, Y. Mu, Y. Huo, Y. Tsuchido, K. Zhu, Sulphur-embedded hydrocarbon belts: Synthesis, structure and redox chemistry of cyclothianthrenes, *Angew. Chem. Int. Ed.* 60 (2021) 18443–18447 (2021). doi:10.1002/anie.202104054.
- [21] D. Ajami, O. Oeckler, A. Simon, R. Herges, Synthesis of a Möbius aromatic hydrocarbon, *Nature* 426 (2003) 819–821 (2003). doi:10.1038/nature02224.
- [22] Virtual NanoLab - Atomistix ToolKit. QuantumWise. v2017.1 (2017).
- [23] C. Bannwarth, E. Caldeweyher, S. Ehlert, A. Hansen, P. Pracht, J. Seibert, S. Spicher, S. Grimme, Extended tight-binding quantum chemistry methods, *WIREs Comput. Mol. Sci.* 11 (2020) e1493 (2020).

doi:10.1002/wcms.1493.

- [24] C. Bannwarth, S. Ehlert, S. Grimme, GFN2-xTB—an accurate and broadly parametrized self-consistent tight-binding quantum chemical method with multipole electrostatics and density-dependent dispersion contributions, *J. Chem. Theory Comput.* 15 (2019) 1652–1671 (2019). doi:10.1021/acs.jctc.8b01176.
- [25] T. Koopmans, Über die zuordnung von wellenfunktionen und eigenwerten zu den einzelnen elektronen eines atoms, *Physica* 1 (1933) 104–113 (1933).
- [26] J. Luo, Z. Q. Xue, W. M. Liu, J. L. Wu, Z. Q. Yang, Koopmans’ theorem for large molecular systems within density functional theory, *J. Phys. Chem. A* 110 (2006) 12005–12009 (2006).
- [27] U. Salzner, R. Baer, Koopmans’ springs to life, *J. Chem. Phys.* 131 (2009) 231101 (2009).
- [28] T. Tsuneda, J. W. Song, S. Suzuki, K. Hirao, On Koopmans’ theorem in density functional theory, *J. Chem. Phys.* 133 (2010) 174101 (2010).
- [29] J. F. Janak, Proof that $\partial E/\partial n_i = \varepsilon_i$ in density-functional theory, *Phys. Rev.* 1978 (18) 7165–7168 (18).
- [30] C. G. Zhan, J. A. Nichols, D. A. Dixon, Ionization potential, electron affinity, electronegativity, hardness, and electron excitation energy: Molecular properties from density functional theory orbital energies, *J. Phys. Chem. A* 107 (2003) 4184–4195 (2003).
- [31] R. G. Parr, L. V. Szentpály, S. Liu, Electrophilicity index, *J. Am. Chem. Soc.* 121 (1999) 1922–1924 (1999).
- [32] W. Humphrey, A. Dalke, K. Schulten, VMD: Visual molecular dynamics, *Journal of Molecular Graphics* 14 (1996) 33–38 (fe 1996). doi:10.1016/0263-7855(96)00018-5.
- [33] L. Wirtz, A. Rubio, R. A. de la Concha, A. Loiseau, *Ab initio* calculations of the lattice dynamics of boron nitride nanotubes, *Phys. Rev. B* 68 (2003) 045425 (2003). doi:10.1103/PhysRevB.68.045425.
- [34] B. Singh, G. Kaur, P. Singh, K. Singh, B. Kumar, A. Vij, M. Kumar, R. Bala, R. Meena, A. Singh, A. Thakur, A. Kumar, Nanostructured boron nitride with high water dispersibility for boron neutron capture therapy, *Sci. Rep.* 6 (2016) 35535 (2016). doi:10.1038/srep35535.
- [35] H. Harrison, J. T. Lamb, K. S. Nowlin, A. J. Guenther, K. B. Ghiassi, A. D. Kelkar, J. R. Alston, Quantification of hexagonal boron nitride impurities in boron nitride nanotubes *via* FTIR spectroscopy, *Nanoscale Adv.* 1 (2019) 1693–1701 (2019). doi:10.1039/c8na00251g.
- [36] H. Zhang, B.-G. Shin, D.-E. Lee, K.-B. Yoon, Preparation of PP/2D–nanosheet composites using *MoS₂/MgCl₂*– and *BN/MgCl₂*–bisupported Ziegler–Natta catalysts, *Catalysts* 10 (2020) 596 (2020). doi:10.3390/catal10060596.
- [37] A. B. D. Nandiyanto, R. Oktiani, R. Ragadhita, How to read and interpret FTIR spectroscopy of organic material, *Indones. J. Sci. Technol.* 4 (2019) 97–118 (2019). doi:10.17509/ijost.v4i1.15806.
- [38] G. Zhang, C. Musgrave, Comparison of DFT methods for molecular orbital eigenvalue calculations, *J.*

Phys. Chem. A 111 (2007) 1554–1561 (2007).

- [39] R. G. Parr, R. G. Pearson, Absolute hardness: companion parameter to absolute electronegativity, J. Am. Chem. Soc. 105 (1983) 7512–7516 (1983).

Supplementary material: Electronic and structural properties of Möbius boron–nitride and carbon nanobelts

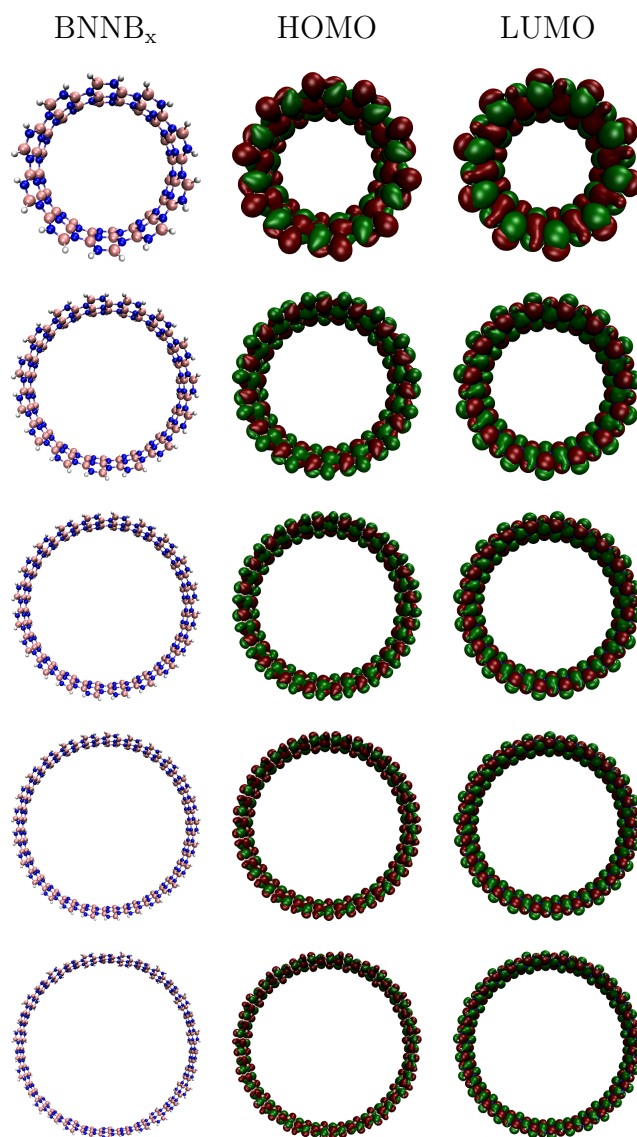


Figure S1: Frontier orbitals (HOMO and LUMO) for all boron–nitride nanobelts. Top to bottom: number of repetitions from 10 to 30.

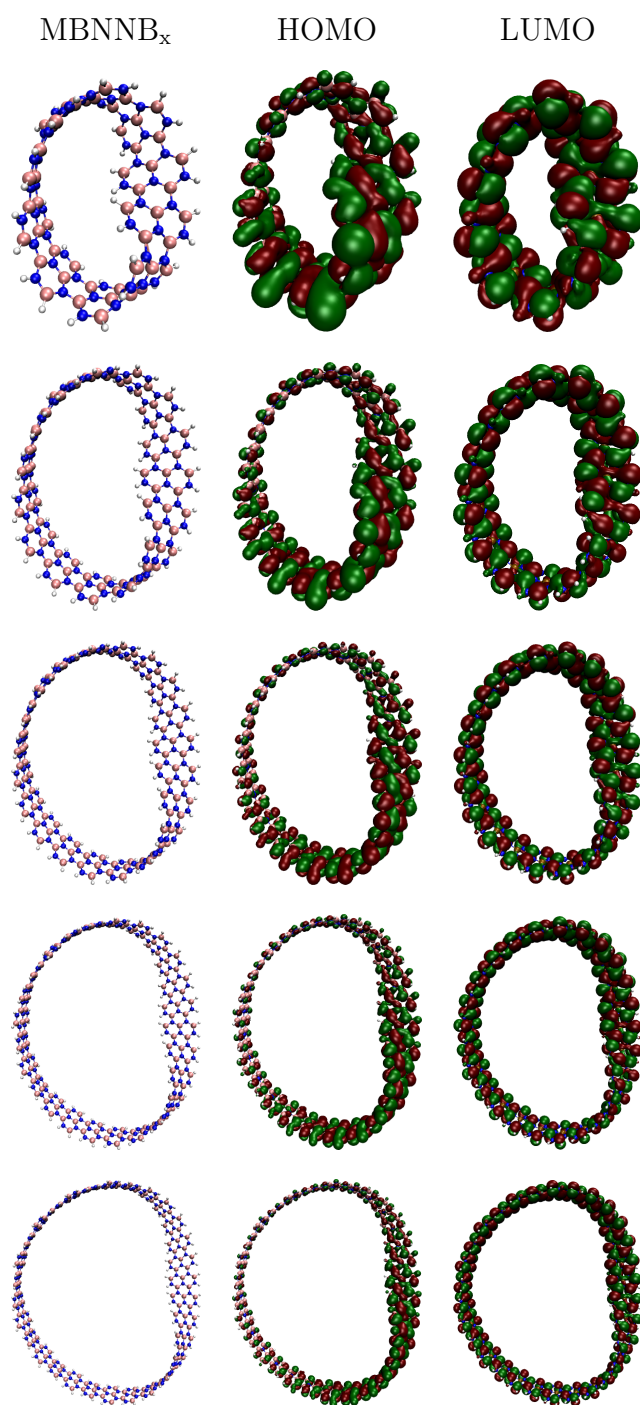


Figure S2: Frontier orbitals (HOMO and LUMO) for all Möbius boron–nitride nanobelts. Top to bottom: number of repetitions from 10 to 30.

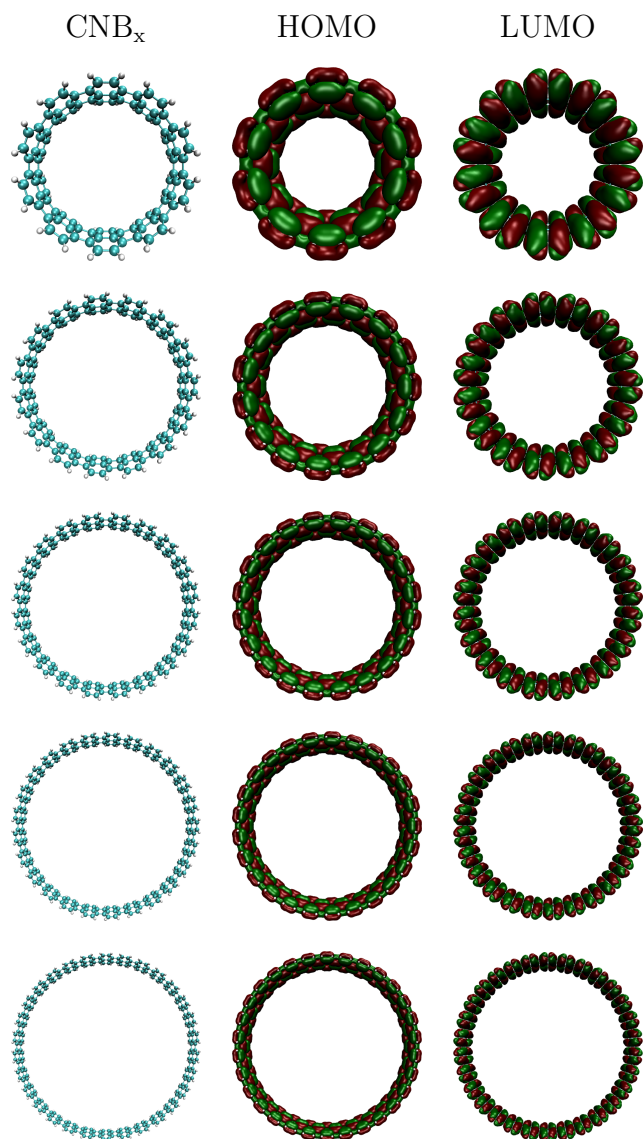


Figure S3: Frontier orbitals (HOMO and LUMO) for all carbon nanobelts. Top to bottom: number of repetitions from 10 to 30.

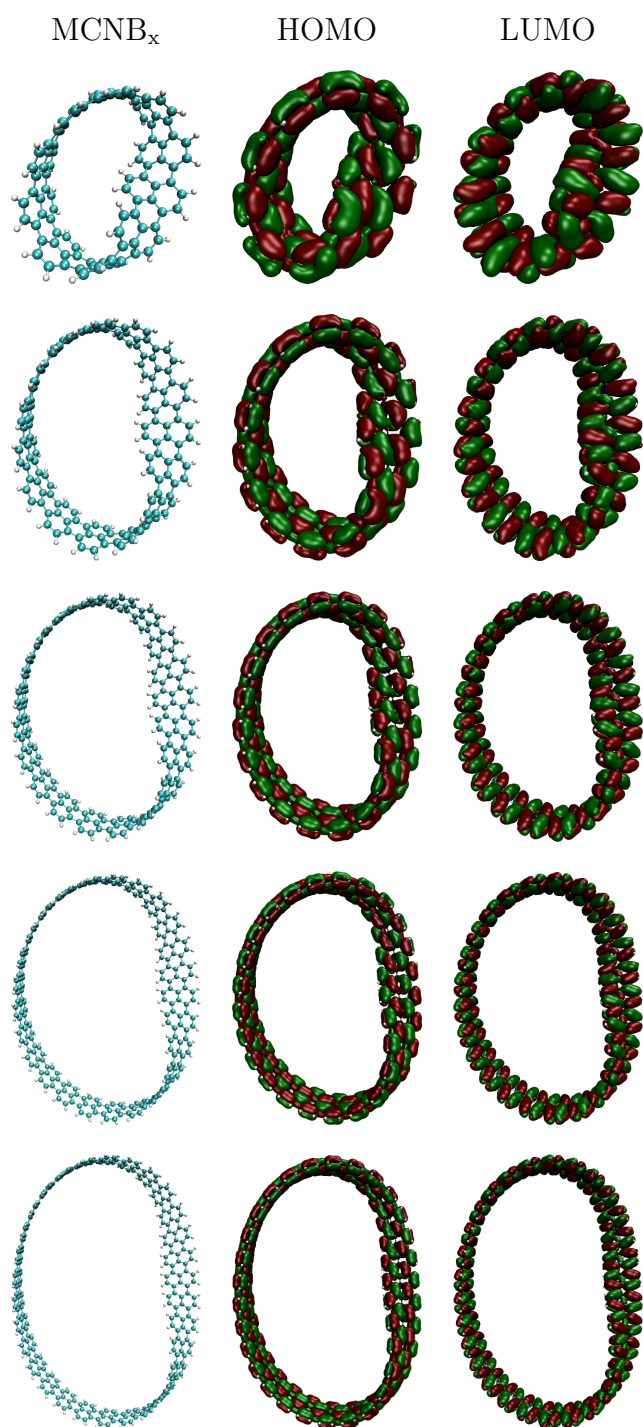


Figure S4: Frontier orbitals (HOMO and LUMO) for all Möbius carbon nanobelts. Top to bottom: number of repetitions from 10 to 30.